Computational Materials Science 187 (2021) 110124

Contents lists available at ScienceDirect

Computational Materials Science

journal homepage: www.elsevier.com/locate/commatsci

Molecular dynamics simulations of spontaneous and seeded nucleation and theoretical calculations for zinc selenide

Leila Separdar [a,*], José Pedro Rino [a], Edgar Dutra Zanotto [b]

[a] Department of Physics, Federal University of São Carlos, Via Washington Luis, km. 235, 13.565-905 São Carlos, SP, Brazil
[b] Department of Materials Engineering, Federal University of São Carlos, Via Washington Luis, km. 235, 13.565-905 São Carlos, SP, Brazil

ARTICLE INFO

Keywords:
Nucleation
Crystal growth
Supercooled liquid
ZnSe
Molecular dynamics simulation
Seeding method
Mean lifetime passage method
Classical nucleation theory

ABSTRACT

Understanding and controlling the liquid to crystal transformation is a central topic for numerous natural phenomena and technological applications. However, the microscopic mechanism of crystal nucleation is still elusive, which leads to strong controversies regarding the ability of the most used model, the Classical Nucleation Theory (CNT), to describe nucleation rates in supercooled liquids. In this work, we were able to deeply supercool Zinc Selenide (ZnSe), and determine spontaneous homogeneous steady-state nucleation rates, J_{MD}, by MD simulations using the mean lifetime method. At moderate supercoolings, where the nucleation rates are much smaller, we used the seeding method to compute the nucleation rates by the CNT formalism, J_{CNT}, without any fitting parameter, using the physical properties obtained by MD simulations: the melting temperature, T_m, density, melting enthalpy, diffusion coefficient, D^+, and the critical nucleus size, N^*, combined with two expressions for the thermodynamic driving force, $\Delta\mu$. The values of interfacial free energy, γ, calculated by the CNT expression using the MD simulation data, via both the seeding method and the mean lifetime method at moderate and deep supercoolings show a weak temperature dependence, which is in line with the Diffuse Interface Theory. The extrapolated values of γ, from the spontaneous nucleation regime to the seeding nucleation region cover the range of values of γ calculated via the seeding method and the CNT formalism. Finally, the J_{CNT} extrapolated from moderate supercoolings to deep supercoolings are in good agreement with the J_{MD}. These results confirm the validity of the CNT.

1. Introduction

The liquid to crystal transition is a ubiquitous phenomenon, which is a very important scientific and technological subject in diverse fields, such as biology, mineral formation, semiconducting materials, water and metal solidification, glass-ceramics and glass formation. The first step of crystallization is the birth of critical nuclei. Their size, structure and rate at which critical nuclei appear and grow are fundamental parameters for understanding and controlling crystallization. Although nucleation rates, $J(T)$, can be measured experimentally in a few systems due to the very small nucleus size (nm) and either a too short or too long lifetime, it is extremely difficult to understand and describe the microscopic mechanism of nucleation, which remains elusive. To this end, computer simulation techniques provide, in principle, a suitable tool to dig deeper into this process. At least three main methods are available to obtain crystal nucleation rates via molecular dynamics simulation (MD): 1) the mean lifetime method [1], 2) enhanced-sampling methods [2,3,4,5,6], and 3) the seeding method [7,8,9,10]. We will use methods 1 and 3 in this study.

The Classical Nucleation Theory (CNT) [11,12] is one of the most well-known models to describe the nucleation process. This theory assumes that the formation of crystal nuclei takes place as a result of thermal fluctuations in a supercooled liquid (SCL). If an embryo overcomes a certain threshold size, N^*, it becomes a critical nucleus that spontaneously grows until it meets other growing crystals otherwise the liquid solidifies. On the other hand, fluctuations below the critical size decay by dissolving back into the supercooled liquid. According to this theory, the interplay between the supercooled liquid/nucleus interfacial free energy, γ, and the difference between the chemical potentials of the crystal phase and the supercooled liquid, $\Delta\mu$, describes the thermodynamics of crystal nucleation. Finally, a third key property is the effective diffusion coefficient, which controls the atomic transport rate at the liquid/crystal interface, $D(T)$. The independent determination of these three quantities allows CNT calculations and comparison with

* Corresponding author.
E-mail address: separdar.leila@gmail.com (L. Separdar).

https://doi.org/10.1016/j.commatsci.2020.110124
Received 23 September 2020; Received in revised form 13 October 2020; Accepted 14 October 2020
Available online 16 November 2020

experimentally determined or simulated nucleation rates. This endeavor has been a theme of several papers, which owing to the scarcity of direct measurements of these properties, often questioned the validity and accuracy of the CNT. Hence, knowledge of these fundamental parameters is a necessary step to test CNT or any other nucleation theory [13]. Unfortunately, very few studies have assessed all of them to allow a rigorous evaluation of the theoretical model.

Previous works have been carried out to test the CNT by molecular dynamics simulations, covering from idealized toy models, such as Lennard-Jones by different methods [10,14,15,16,17,18,19], and hard sphere colloids [20] to realistic models of real substances, for instance H_2O [21,22], SiO_2 [23], NaCl [24,25], Ge [26], BaS [27], $Ni_{50}Ti_{50}$ [28] and Ni [29]. In all the above-mentioned papers, the CNT predictions were (more or less) validated by MD simulations. However enormous discrepancies of 10 to 50 orders of magnitude were found when nucleation rates calculated by the CNT formalism were compared with actual laboratory experiments with glass forming substances, e.g., as referred to in [30,31,32]. In these experimental studies, the diffusion coefficients, D, were estimated via the liquid viscosity and the interfacial free energy, γ, was left as a (constant) fitting parameter. Some authors related this huge discrepancy to the absence of a direct way of measuring these key parameters (D and γ) and also CNT intrinsic limitations; for example the assumption that a critical nucleus of molecular size has macroscopic bulk-size properties and that the liquid/nucleus interface is sharp, even though the nanosized critical cluster may be almost purely "interface" [13]. Hence, the validity of the CNT remains an open problem that warrants further detailed work.

For most substances, it is very difficult to detect (by actual experiments or simulations) spontaneous homogeneous nucleation, however in some supercooled liquids, homogenous nucleation occurs naturally within reasonable MD simulation time scales with nucleation rates of $(10^{30}-10^{35})m^{-3}s^{-1}$ [16,19,23,33,34,35,36]. The study of such unique systems provides a great opportunity to test the limits of validity and applicability of the CNT and other theories. Here, we are interested in comparing nucleation rates calculated using CNT, with values found directly from a substance that spontaneously crystallizes in MD simulation time scales. Some simulation studies have compared the calculated nucleation rates with values determined independently by MD [16,23,24,36,37,38]. These comparisons provide a key tool for developing, testing, and perhaps improving theoretical descriptions of nucleation. To examine the validity of the CNT, in this work we obtained the steady-state nucleation rates, $J_{ss}(T)$, for Zinc Selenide (ZnSe) using the mean lifetime method. We have also calculated the nucleation rates using the CNT and physical properties obtained by MD via the seeding method. Jointly, these two MD methods covered a supercooling range $(0.7-0.9)T/T_m$.

The substance chosen in this study, ZnSe, is very important in optics [39,40]. This material is a type II-VI semiconductor with a wide-bandgap, which can be made in both hexagonal (wurtzite) and zinc-blende structures, and many attempts have been made to understand its structure, optical and electronic properties experimentally, for example [41,42,43]. Therefore, further knowledge of physical properties and kinetic behavior of ZnSe could be meaningful. However, this is not the focus of this work. Here, due to the fact that homogeneous nucleation can be detected in MD timescales using a robust potential, we use this substance as a model to investigate the *validity of the CNT* by comparing calculated nucleation rates with values of spontaneous nucleation obtained by MD.

The paper is organized as follows. In the next section, we describe the theoretical background, Section 3 describes the simulation details of the substance ZnSe, and in Section 4 we present the results obtained for the melting temperature, density, critical nucleus sizes, interfacial free energy and nucleation rates. We then use these data to calculate nucleation rates by CNT and compare them with the MD nucleation rates. Finally, in Section 5, we discuss and summarize the main results.

2. Theoretical background

According to the Classical Nucleation Theory [11,12], in a supercooled liquid system at constant temperature, T, and pressure, p, the appearance of a crystal cluster requires a Gibbs free energy change or work of formation, given by

$$\Delta G(N) = -N\Delta\mu + \gamma A \tag{1}$$

where N is the number of particles in the crystal cluster, $\Delta\mu$ is the chemical potential difference between the supercooled liquid and the crystal phase, $G_{scl}-G_{crystal}$, which is positive, γ is the crystal-liquid interfacial free energy, and A is the cluster surface area. In this equation, the strain energy term is neglected due to its (assumed) fast relaxation in the supercooled liquid.

The function $\Delta G(N)$ goes through a maximum at

$$\Delta G^* = N^*\Delta\mu/2 \tag{2}$$

where N^* is the number of atoms in the critical nucleus. If the cluster shape is spherical, then:

$$N^* = \frac{32\pi\gamma^3}{3\rho_s^2\Delta\mu^3} \tag{3}$$

where ρ_s is the number of atoms per unit volume in the critical crystal nucleus; its unit is A^{-3}. This density is supposed to be equal to the density of the crystal at the same temperature.

The steady-state nucleation rate, $J_{ss}(T)$, i.e., the average number of viable crystal nuclei formed per unit time per unit volume is given by the product of: i) the number density of critical clusters, $\rho_f exp[-\Delta G^*/(k_B T)]$, where ρ_f is the number of atoms per unit volume in the supercooled liquid and k_B is the Boltzmann constant and ii) the dimensionless Zeldovich factor $Z^* = \sqrt{\frac{\Delta\mu}{6\pi k_B T N^*}}$ and iii) the attachment rate of the atoms from the liquid to the critical cluster, D^+,

$$J_{ss}(T) = Z^* D^+ \rho_f \exp[\frac{-\Delta G^*}{k_B T}] \tag{4}$$

For most cases, $Z^* = 0.01-0.10$ [12], which characterizes the shallow curvature of the energy barrier at its top, and takes into account the possible dissolution of a fraction of supercritical nuclei. The evaluation of D^+ depends on the choice of the model that describes the process near the surface of the growing crystal nuclei. Therefore, to obtain the theoretical value of $J_{ss}(T)$, we need to know four properties of the system: $\Delta\mu, \rho_f, N^*$ and D^+. Below we explain how each property can be determined by computer simulations.

In the case of isobaric supercooling, $\Delta\mu$ can be well approximated by a widely used expression [44], which gives an upper bound

$$\Delta\mu = \Delta h_m \frac{(T_m - T)}{T_m} \tag{5}$$

or by using an alternative form [45,46,47] if the difference between the specific heats of the liquid and crystal at the melting point, $\Delta c_{p,m}$, is known

$$\Delta\mu = \Delta h_m \frac{(T_m - T)}{T_m}\left[1 - \frac{\Delta c_{p,m}}{\Delta s_m}\frac{(T_m - T)}{2T_m}\right] \tag{6}$$

where T_m is the melting temperature, Δh_m is the melting enthalpy; the difference between the enthalpy of the liquid and crystal at the melting temperature, Δs_m is the melting entropy, which is related to Δh_m by $\Delta s_m = \Delta h_m/T_m$. In this article, we used both expressions (5) and (6) for calculating $\Delta\mu$.

The number density of the fluid, ρ_f, and crystal, ρ_s, can be calculated from an ensemble average in an NpT simulation at any specific temperature.

Evaluation of N^* depends on the technique used. In the seeding method, its value is pre-known. A crystalline cluster of given shape, structure and number of atoms is inserted in the supercooled fluid. Otherwise, determination of N^* according to Eq. (3) needs the knowledge of γ, $\Delta\mu$ and ρ_s.

It is quite difficult to measure γ experimentally. However, several simulation methods have been implemented for determining γ, such as the mean lifetime method [1], the cleaving method [48], the capillary fluctuation technique [49], metadynamics [50] and umbrella sampling [20]. After determining γ, one can evaluate N^* via Eq. (3). Here we have used both the seeding method and the mean lifetime method.

To obtain D^+, we can use an expression proposed in [51], used e.g. in refs. [10,52]

$$D^+ = \frac{\langle (N(t) - N^*)^2 \rangle}{2t} \tag{7}$$

D^+ can be obtained from the CNT [10]

$$D^+ = \frac{24D(T)\sqrt[3]{N^{*2}}}{\lambda^2} \tag{8}$$

where λ is the distance travelled by the particles in the vicinity of a cluster to attach to its surface, and is expected to be of the same order of magnitude as the unit cell of the crystal phase, in the case of ZnSe $\lambda = 5.643A^o$. $D(T)$ is the effective diffusion coefficient, which is obtained from the mean square displacements via Einstein's equation, $\langle r^2(t) \rangle = 6Dt$.

In the seeding method, after determining all parameters explained above, one can introduce them into Eq. (4) to calculate the nucleation rates for some thermodynamic state points, and also to extrapolate the $J_{ss}(T)$ outside the temperature range where the calculations were performed.

In situations when spontaneous nucleation can be detected by MD for reasonable computational times, we can use the mean lifetime method [1] to determine nucleation rates to determine nucleation rates as it was previously done for instance in Ref. [27]. In this technique, by estimating the average time of the birth of the first nucleus, τ, and using the definition $J_{MD} = 1/(\tau V)$, where V is the volume of the system, one can calculate the nucleation rate for some thermodynamic state points, and then analyze the MD results for J_{MD} by the CNT. By substituting Eq. (3) and Eq. (8) into Eq. (4) the CNT equation becomes [53]

$$J_{ss} = \sqrt{\frac{\gamma}{k_B T}} \frac{D(T)}{\lambda^4} \exp\left[\frac{-16\pi\gamma^3}{3k_B T {\rho_s}^2 \Delta\mu^2}\right] \tag{9}$$

With this equation we can estimate the average value of interfacial free energy, γ, from the slop of a plot of $Ln[\frac{J\sqrt{T}}{D(T)}]$ versus $1/(T{\rho_s}^2\Delta\mu^2)$ [53]. Another way to find the temperature dependence of γ is to substitute the values of J_{MD}, T, $D(T)$, $\Delta\mu$, λ and ρ_s into Eq. (9) and solving the equation to evaluate γ for each thermodynamic state point and then fit these values to find the temperature dependence of $\gamma(T)$. By knowing the average value of γ, or its temperature dependence at deep supercoolings, one can extrapolate $J_{MD}(T)$ to the moderate supercooling region where nucleation rates were estimated by the seeding method. Thus, we can compare the extrapolated nucleation rates in the deep supercooling regime (spontaneous nucleation) with those obtained in the moderate supercooling regime (seeded nucleation).

3. Simulation details

In this work, we developed an effective inter-atomic potential consisting of two-body and three-body interactions to describe the kinetics of crystal nucleation and growth in supercooled ZnSe:

$$V = \sum_{i<j=1}^{N} {V_{ij}}^{(2)}(r_{ij}) + \sum_{i,j<k=1}^{N} {V_{jik}}^{(3)}(r_{ij}, r_{ik}) \tag{10}$$

The two-body term includes 4 terms: steric repulsion, coulomb interaction due to charge transfer between ions, charge-induced dipole attractions due to the electronic polarizability of anions, and van der Waals attraction, which is given by the equation:

$$V_{ij}^{(2)}(r) = \frac{H_{ij}}{r^{\eta_{ij}}} + \frac{Z_i Z_j}{r} e^{-r/\lambda} - \frac{D_{ij}}{2r^4} e^{-r/\xi} - \frac{W_{ij}}{r^6} \tag{11}$$

Here H_{ij} is the intensity of the steric repulsion, Z_i is the effective charge of the ions, in units of the electronic charge $|e|$. η is the exponent of the steric repulsion, λ and ξ are the coulomb and charge-dipole interaction screening lengths respectively. $D_{ij} = \alpha_i {Z_j}^2 + \alpha_j {Z_i}^2$, α_i is the electronic polarizability of ions. Finally, W_{ij} is the strength of the dipole–dipole attractions.

The three-body effective interaction potential is given by a product of spatial and angular dependence to describe bond bending and bond stretching correctly.

$$V_{jik}^{(3)}(r_{ij}, r_{ik}) = R^{(3)}(r_{ij}, r_{ik}) P^{(3)}(\theta_{jik}) \tag{12}$$

where

$$R^{(3)}(r_{ij}, r_{ik}) = B_{jik} \exp\left(\frac{\gamma}{r_{ij} - r_0} + \frac{\gamma}{r_{ik} - r_0}\right) \Theta(r_0 - r_{ij}) \Theta(r_0 - r_{ik}) \tag{13}$$

$$P^{(3)} = \frac{(cos\theta_{jik} - cos\bar{\theta}_{jik})^2}{1 + C_{jik}(cos\theta_{jik} - cos\bar{\theta}_{jik})^2} \tag{14}$$

B_{jik} is the strength of the interaction, θ_{jik} the angle formed by $\vec{r}_{ij}$ and $\vec{r}_{ik}$, $\bar{\theta}_{jik}$ and C_{jik} are constant, and $\Theta(r_0 - r_{ij})$ is the step function. The potential was parameterized in a way that the cohesive energy at $T = 0K$, density, bulk modulus, the C_{11} elastic constant, the vibrational density of states and the specific heat of ZnSe were reproduced with this potential and were in agreement with experimental results from [54,55,56]. The potential parameters are listed in Table 1. All parameters for interactions of Zn-Zn-Se, Zn-Se-Zn, Se-Zn-Se and Se-Se-Zn were set to zero. All simulations were done in NpT and NVT ensembles. The LAMMPS package [57], was used for the simulations. The timestep was 1.0 *fs*. Nose-Hoover thermostat and barostat were used to control the temperature and pressure. Periodic boundary conditions were applied in all directions. The potential was truncated at $r = r_c = 6.2\ A^o$.

In the next section, we explain the MD results of melting temperature, diffusion coefficient, the critical nucleus size, the thermodynamic driving force and densities.

4. Simulation results

4.1. Determining the melting temperature

Knowledge of the melting point is the first step towards the CNT

Table 1
The values of potential parameters used in our simulations of ZnSe.

	Zn-Zn-Zn	Se-Se-Se	Zn-Se-Se	Se-Zn-Zn
$H(eV.A^{*\eta})$	82.800611	3291.461985	3981.333767	3981.333767
η	7	7	9	9
Z_i	0.8261	−0.8261	0.8261	−0.8261
Z_j	0.8261	−0.8261	−0.8261	0.8261
$\lambda(A^o)$	5.0	5.0	5.0	5.0
$D(eV.A^{*4})$	0.0	39.362098	19.681049	19.681049
$\xi(A^o)$	3.75	3.75	3.75	3.75
$W(eV.A^{o6})$	0.0	0.0	355.547483	355.547483
$B(eV)$	0.0	0.0	1.7540574	1.7540574
$\gamma(A^o)$	0.0	0.0	1.0	1.0
$r_0(A^o)$	0.0	0.0	3.8	3.8
C	0.0	0.0	6.00	6.00
$\cos(\theta)$	0.0	0.0	−0.333333	−0.3333333

investigation. For this task, a zinc-blend structure of ZnSe was created in a cubic box of 56.43Å in length. The total number of atoms was 8,000. We determined the melting temperature T_m at $p = 0$ *bar*, with two different approaches. We analyzed both mechanical and thermodynamic melting temperatures of ZnSe.

4.1.1. Mechanical melting point

To determine the mechanical melting point, we started by equilibrating the crystalline phase at $T = 300K$ and pressure$p = 0$ *bar*, then the system was heated up to $2500K$ and cooled down to the initial temperature with the same heating/cooling rate ranged from 10 to $0.1K/ps$. Fig. 1 shows the potential energy per particle as a function of temperature for three different heating/cooling rate. During the heating process, a sudden jump in potential energy occurs at superheating temperature T_+ and during the cooling, there is a drop in potential energy at supercooling temperatureT_-. From the magnitude of superheating and supercooling temperatures, one can estimate the mechanical melting temperature by the equation [58,59]:

$$T_m = T_+ + T_- - \sqrt{T_+ T_-} \tag{15}$$

The best estimate for this temperature is $T_m \cong 1357K$ at the lowest cooling rate 0.1K/ps. The value of T_m calculated by this method relates to the cooling rate. The potential energy-temperature curve reveals the effect of the heating/cooling rate on the determination of melting temperature by the hysteresis method. Hence, it is important to choose a more precise method.

4.1.2. Thermodynamic melting point

In comparison to the hysteresis approach, the standard phase-coexistence technique used in refs. [60,61,62] has more physical meaning. In this approach, we discover the temperature, at which the solid–liquid interface coexists, this condition occurs when the free energy of solid and liquid states becomes equal. To do so, we prepared a supercell containing $10 \times 10 \times 30$ unit cells of ZnSe (24,000 atoms) and heated it up to $T = 1300K$ at $p = 0$ *bar*. Then the supercell was divided into two parts in the z direction. One half of the atoms in the supercell was kept fixed at $T = 1300K$ and the other half was heated up to a higher temperature (such as $T = 2500K$ which is above the experimental melting temperature $T_{m,exp} = 1800K$ [63]) at $p = 0bar$ to create a liquid phase. The liquid part is then cooled down to temperature $T = 2000K$ (close to $T_{m,exp} = 1800K$ but still higher than the expected melting temperature). The result of this process was a supercell containing solid at $T = 1300K$ in one half, and liquid at $T = 2000K$ in the other.

The two-phase supercell prepared was heated by MD runs in the NpT ensemble and temperature T was increased from $1300K$ to $2000K$ in $50K$ intervals. At each temperature, the system was left to evolve for $t = 1ns$ and the phase change of the box was visually monitored. Fig. 2 shows the potential energy per particle as a function of time at seven selected temperatures above and below T_m. At $T < 1350K$, the system crystallized and simultaneously the potential energy decreased, where for $T > 1400K$, the liquid phase progressed and the system melted rising the potential energy. Next the initial two-phase supercell was heated from $1400K$ to $1350K$ in $10K$ intervals and after that in $2K$ intervals to determine the melting point more precisely. At $T = 1388 \pm 2K$, which is called the melting point, the solid–liquid interface remains stationary. This value is $30K$ above the mechanical melting point and $412K$ below the experimental melting point. $T_m = 1388 \pm 2K$ will be used as the melting point throughout this paper.

4.2. Nucleation rates calculated via the seeding method

To prepare the configuration of an amorphous matrix containing an artificially created crystalline nucleus, first a supercell containing $13 \times 13 \times 13$ unit cells, equivalent to 17,576 atoms at $T = 300K$, was equilibrated. Then, the crystal seed was heated up to $T = 1000K$, which is below its melting temperature. In the geometrical center of the hot crystal, a sphere region with a certain radius was defined. Therefore, initially, the spherical seed and the matrix around it have the same structure and lattice parameter initially. Finally, the matrix was heated up to $T = 2000K$ to liquefy, while the atoms in the solid sphere were kept fixed at their positions. Finally, the matrix was cooled down below the equilibrium melting temperature by a cooling rate of $1K/ps$. Thus, we constructed a supercooled liquid containing a crystal seed of radius R^*.

4.2.1. The coexistence (critical) temperature

After preparing the system (matrix + seed); we found the coexistence (critical) temperature, T^*, at which, the seed started to grow in the supercooled liquid. For reliable statistics, fifteen independent configurations of the matrix containing the same nucleus size were studied. Owing to the fact that the equilibrium between the nucleus and its surrounding metastable phase was unstable, finding the coexistence temperature became difficult. Hence, we defined the coexistence temperature as the temperature at which the seed grows in seven or eight of the fifteen independent configurations and fully dissolves in remained configurations. This procedure was repeated for six different seed sizes.

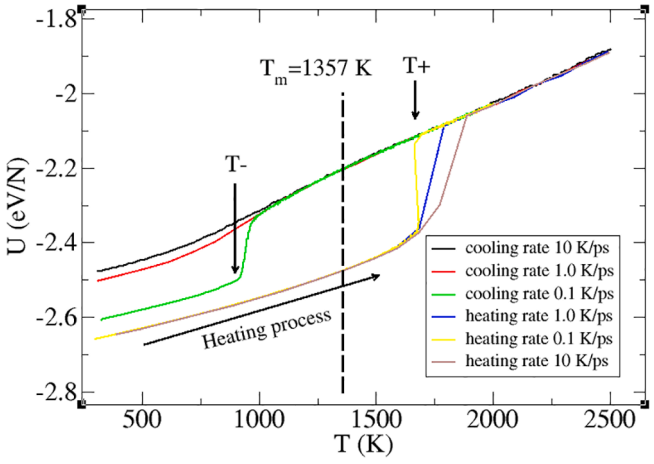

Fig. 1. Potential energy per particle as a function of temperature for three different heating/cooling rates of 10, 1.0 and $0.1K/ps$. The melting temperature can be determined from the superheating temperature T_+ and supercooling temperature T_- using Eq. (15).

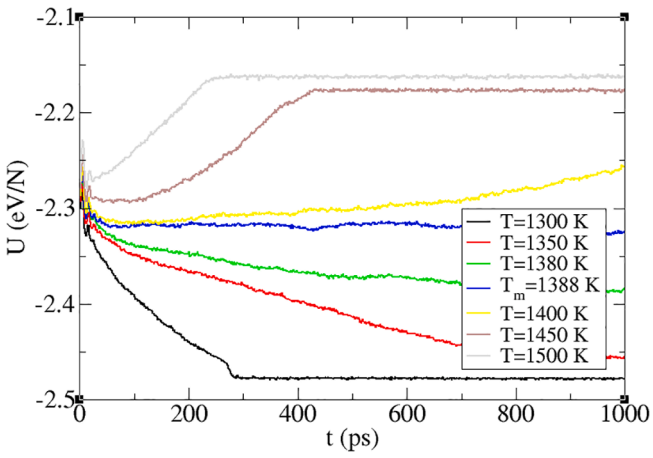

Fig. 2. Potential energy per particle versus time at selected temperatures above and below melting temperature. For temperatures above $T_m = 1388K$, the potential energy increased, whereas for temperatures below it, it decreased. The potential energy is practically constant at the melting point.

Each amorphous matrix + seed was allowed to evolve for $t = 0.5ns$ at each temperature to test if the seed grew or dissolved. During this time interval, solid-like particles in the seed environment were identified by calculating the Steinhardt bond-order parameter [64,65], $S_{ij} = \sum_{m=-6}^{m=+6} q_{6m}(i).q^*_{6m}(j)$, where $q_{6m}(i) = \frac{1}{N_b(i)}\sum_{j=1}^{N_b(i)} Y_{lm}(\vec{r}_{ij})$ is the Steinhardt parameter, $Y_{lm}(\vec{r}_{ij})$ are the spherical harmonics, $N_b(i)$ is the number of nearest neighbors of atom i, $\vec{r}_{ij}$ is the vector connecting it with its neighbors j. If the value of the dot product, $q_6.q_6 > 0.5$, the particle–particle association was considered solid-like [10]. Recently, it was shown that the choice of $N_b(i)$ affects the value of N^* and the nucleation rate [66]. We tested the q_6 results using a set of different numbers of connections at one temperature, to find which is the most appropriate for the crystallization case. In this case, if a particle is involved in more than eleven solid-like associations, it was considered to be in the seed environment. Details about how one can determine the number of connections are provided in ref. [64].

A good criterion to determine the growth of a crystalline seed is the time evolution of the potential energy $U(t)$, or enthalpy. A sharp decrease in potential energy indicates seed growth and the beginning of a phase transition. If $U(t)$ increases or remains approximately unaltered, this means that the seed dissolved. Fig. 3 shows the time evolution of the potential energy per particle for two independent configurations with the same seed size $N = 442$ particles, at $T = 1235K$. In curve (1) the seed has dissolved, whereas in curve (2) the seed has grown. The inset shows the time evolution of the number of particles in the seed, determined by the q_6 method.

Regarding the $U(t)$, the critical temperatures at which the seed has an equal probability of growth and dissolution were determined for six different seed sizes. Fig. 4 shows the number of atoms in the critical crystal seed, N^*, as a function of temperature. The critical size, N^*, decreases monotonically from $N^* = 642$ to $N^* = 59$ with decreasing temperature, as expected from the CNT. From N^* and the density of crystal at the critical temperatures, $\rho_s(T^*)$, the radius of the critical nucleus at each T^*, $R^* = \left(\frac{3N^*}{4\pi\rho_s(T^*)}\right)^{1/3}$, was calculated. The inset of the Fig. 4 shows the calculated R^* as a function of $\frac{1}{\Delta T} = \frac{1}{(T_m - T)}$. It is obvious that R^* is practically a linear function of the inverse temperature, in accordance with the CNT prediction and the MD results reported in Refs. [26,52].

4.2.2. The thermodynamic driving force

As discussed in Section 2, another quantity that must be determined for testing the CNT is the difference between the chemical potentials of liquid and crystal, $\Delta\mu$. In this study, $\Delta\mu$ was calculated by Eq. (5) and Eq.

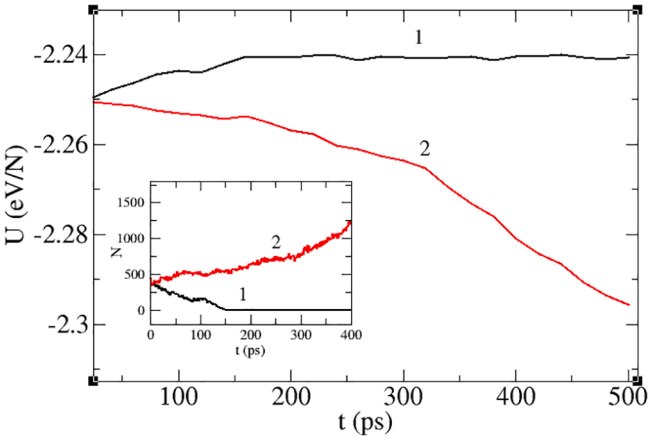

Fig. 3. Time evolution of the potential energy of the system (supercooled liquid + seed) at ($T = 1235K$). In (1), the seed dissolves, whereas in (2), the seed grows. The inset shows the time evolution of the number of particles in the seed for each configuration.

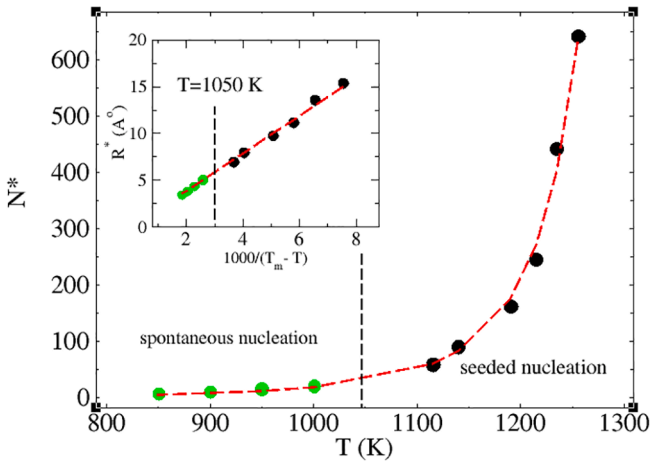

Fig. 4. Number of atoms in the critical crystal nucleus, N^*, as a function of temperature. T^* was obtained from the seeded nucleation simulations. By substituting the $\rho_s(T)$, $\Delta\mu(T)$ from Eq. (5) and $\gamma(T)$ from the linear fit of $\gamma(T^*)$ into Eq. (3), N^* was extrapolated to the region where spontaneous nucleation occurs. The red dashed line refers to this extrapolation. The vertical dashed line separates the seeded from the spontaneous nucleation regime. The inset shows the radius of the critical nucleus, R^*, as a function of $\frac{1}{(T_m - T)}$. The black circles in the inset refer to the R^* calculated from $R^* = (\frac{3N^*}{4\pi\rho_s(T^*)})^{1/3}$ at each critical temperature. The red dashed line in the inset refers to the R^* extrapolated to the deep supercooling regime by substituting the values of $\rho_s(T)$ and the extrapolated $N^*(T)$ into $R^* = (\frac{3N^*(T)}{4\pi\rho_s(T)})^{1/3}$. The green circles refer to R^* and N^*, which were calculated from $R^* = 2\gamma/(\rho_s\Delta\mu)$ and $N^* = \rho_s(4\pi R^{*3}/3)$, respectively, using the mean lifetime method. Here γ was calculated from Eq. (9) by inserting the J_{MD}, T_m, λ, $D(T)$ and $\Delta\mu(T)$ into Eq. (9).

(6) using the MD results of $T_m = 1388K$, $\Delta h_m = 0.266ev/atom$ and $\Delta c_{p,m} = 5.4 \times 10^{-5} ev/K$. The results of $\Delta\mu$ are shown in Table 2. There is no significant difference between the values of $\Delta\mu$ calculated by the two equations. To calculate $\Delta c_{p,m}$, we plotted the enthalpy as a function of temperature during the heating and cooling process with the rate $1K/ps$ explained in Section 4.1.1. A numerical derivation of each heating/cooling curve, $\frac{dh}{dT}$, gives the temperature dependence of $c_p(T)$ in the crystal and liquid phases. The difference between the specific heat of crystal and liquid at melting temperature, $\Delta c_{p,m} = c_{p,liq}(T_m) - c_{p,crystal}(T_m)$ gives us $\Delta c_{p,m} = 5.4 \times 10^{-5} ev/K$.

4.2.3. The number density of crystal and liquid at critical temperatures

After determining the critical temperatures, T^*, at which the seeds have an equal probability of growth and dissolution, we obtained the

Table 2
Values of the quantities used for the calculation of $J(T)$ via the seeding technique.

N^*	642	442	245	162	91	59
$T^*(K)$	1255(5)	1235(5)	1215(5)	1190(5)	1140(5)	1115(5)
$D^+(ps^{-1})$	60.90	51.28	28.96	26.93	24.10	9.35
$\rho_f(A^{o-3})$	0.0334	0.0336	0.0338	0.0341	0.0348	0.0351
$\rho_s(A^{o-3})$	0.0416	0.0417	0.0418	0.0418	0.0420	0.0421
$\Delta\mu(eV)$ (Eq. (5))	0.0254	0.0293	0.0331	0.0379	0.0475	0.0523
$\Delta\mu(eV)$ (Eq. (6))	0.0251	0.0288	0.0325	0.0371	0.0463	0.0508
$\gamma(J/m^2)$	0.130	0.129	0.128	0.127	0.124	0.123
$J(m^{-3}s^{-1})$	3.5E + 07	9.17E + 13	2.27E + 23	1.76E + 27	6.68E + 30	1.18E + 33

values of $\rho_s(T^*)$ and $\rho_f(T^*)$ in each of them using an NpT ensemble in a system of $N = 8,000$ atoms. Starting from the crystalline state at $T = 300\ K$, we heated up the system at 1 K/ps to reach the target critical temperatures $T^* = 1115, 1140, 1190, 1235$ and $1255K$ in a crystalline state. At each temperature, the system was first equilibrated for $t = 0.1ns$. Afterwards, the average density was calculated during another $t = 0.5ns$. The last studied thermodynamic state of the crystal was then heated up with the same heating rate until the crystal completely liquified. Then the liquid was cooled down to temperatures $T^* = 1255, 1235, 1190, 1140, 1115K$ with the same rate and again after equilibrating the system at each temperature ρ_f averaged over 0.5 ns. The results of the number densities of crystal and liquid at critical temperatures were reported in Table 2.

4.2.4. The interfacial free energy

By substituting the MD data for N^*, $\rho_s(T^*)$ and $\Delta\mu(T^*)T^*$ into Eq. (3), we calculated the nucleus/liquid interfacial free energy at each temperature T^*. The results are reported in Table 2 and shown in Fig. 9. The values of $\gamma(T^*)$ in the studied temperature interval show a weak temperature dependence which was predicted theoretically [67] and reliably obtained in MD simulations [10,26,52,68]. The average value of calculated γ corresponding to the supercooling range $T = (0.8-0.9)T_m$ is $\gamma_{avg} = 0.127J/m^2$. A linear fit according to $\gamma(T) = aT + b$, to the values of $\gamma(T^*)$ gives us the temperature dependence of γ. By substituting the $\gamma(T)$, $\rho_s(T)$ and $\Delta\mu(T)$ into Eq. (3), we extrapolated N^* to the region where spontaneous nucleation occurs. The result of this extrapolation is shown in Fig. 4 by the red dashed line. Using the seeding method in deep supercoolings would require small number of atoms in seed, $N^* < 18$, which corresponds to a seed with radius$R < 5A^o$, which would lead to large errors associated with incorrectly estimating the number of atoms in the nucleus, due to its numerous surface atoms. In Section 4.3 we will compare these numbers with those calculated from the spontaneous nucleation experiments via the mean lifetime method.

4.2.5. The work of forming a critical nucleus

The work of forming a critical nucleus (or activation barrier) can be obtained from $W^* \equiv \Delta G^* = \frac{N^*\Delta\mu}{2}$ using the MD data of T_m, $\Delta\mu$, Δh_m, $\Delta c_{p,m}$. The calculated (reduced) value of the activation barrier W^*/k_BT varies from 75.6 at $T = 0.9T_m$ to 16.1 at $T = 0.8T_m$. We extrapolated W^*/k_BT to deep supercoolings using the $\Delta\mu(T)$ from Eq. (6) and the extrapolated $N^*(T)$ explained in Section 4.2.4. The extrapolated values of $\frac{W^*}{k_BT}$ change between $(3.5-7.3)$ for the temperature range $T = (0.61-0.72)T_m$, which is in accordance with the $\frac{W^*}{k_BT}$ calculated in Section 4.3, $\frac{W^*}{k_BT} = 5.5-9.3$. These values of the reduced activation barrier are not far from that reported for SiO_2 at deep supercoolings $\frac{W^*}{k_BT} = 7.86$ at $T = 3000K$ [23] and for homogeneous crystallization of a Lennard-Jones liquid, $\frac{W^*}{k_BT} = 11-22$ [18].

We also calculated the Zeldovich factor, Z^*, using the relation $Z^* = \sqrt{\frac{\Delta\mu}{6\pi k_B T N^*}}$ in conjunction with Eq. (5). We found it increases from 0.004 at $T = 0.9T_m$ to 0.02 at $T = 0.8T_m$. The use of Eq. (6) for $\Delta\mu$ leads to the same values. The Zeldovich factor is expected to be (10^{-2}). Results of the same order of magnitude were reported in MD simulations of Ge [26], LJ [52] and SiO_2 [23].

4.2.6. The transport coefficient

The transport coefficient at the liquid/nucleus interface was calculated from Eq. (7) and the results were shown in Table 2. During 0.5 ns after the implementation, every $1ps$, the size of the nucleus was calculated by analyzing the atom configurations using the q_6 method [64,65]. We carried out fifteen independent evolutions of the embedded critical crystal in six thermodynamic state points. The slope of the time dependence of $\langle (N(t) - N^*)^2 \rangle$ at each temperature determined the value of D^+. The results from the seeded simulations show that D^+ decreases with supercooling (as expected) and changes by one order of magnitude in the temperature range investigated, as shown in Table 2. The range of D^+, its order of magnitude, is consistent with the typical values observed in MD simulations of crystallization of other simple liquids at similar supercooling [21,23,24,26,52].

4.2.7. Nucleation rates

Finally, combining the MD results for N^*, D^+, ρ_f and $\Delta\mu$ at each critical temperature, T^*, we computed the kinetic pre-factors, $J_0 = Z^*D^+\rho_f$, and the nucleation rates, J_{CNT}, from Eq. (4) at six temperatures $T^* = 1255,\ 1235,\ 1190,\ 1140,\ 1115K$. The calculated kinetic pre-factors vary from $J_0(T^* = 0.9T_m) = 10^{39}m^{-3}s^{-1}$ to $J_0(T^* = 0.8T_m) = 10^{40}m^{-3}s^{-1}$. As expected, the kinetic pre-factor depends only weakly on the temperature.

The nucleation rates, $J_{CNT}(T^*)$, show a variation in the range $(10^7 - 10^{33})m^{-3}s^{-1}$ in the supercooling range of $T = (0.8-0.9)T_m$. Such an enormous change is not surprising because the nucleation rate is expected to increase rapidly with increasing supercooling until the maximum is reached.

After the nucleation rates were calculated from N^*, D^+, ρ_f and $\Delta\mu$ at six different thermodynamic state points, we fitted the nucleation rates with the CNT expression. The idea was to get extrapolate the $J_{CNT}(T)$ outside the temperature range, where the seeding simulations and related calculations were performed.

To do this, we needed to obtain the temperature dependence of N^*, D^+, ρ_f and $\Delta\mu$. To calculate the $\Delta\mu(T)$, we used Eq. (5) or (6). The values of $\rho_f(T)$ and $\rho_s(T)$ were obtained from MD simulations at each temperature, T, according to the procedure explained in Section 4.2.3. To obtain the temperature dependences of $N^*(T)$ we substituted the $\gamma(T)$, $\rho_s(T)$ and $\Delta\mu(T)$ into Eq. (3) as explained in Section 4.2.4. From $N^*(T)$ and $D(T)$ and $\lambda = 5.643A^o$ using Eq. (8) we calculated the $D^+(T)$. With $N^*(T)$, $D^+(T)$, $\rho_f(T)$and $\Delta\mu(T)$, we extrapolated $J_{CNT}(T)$ via Eq. (4). Fig. 5 shows both the calculated $J_{CNT}(T^*)$ (black squares) and the extrapolated$J_{ss}(T)$ (red dashed line). The calculated $J_{CNT}(T)$ and extrapolated nucleation rates, using the more elaborated Eq. (6) to calculate $\Delta\mu$, do

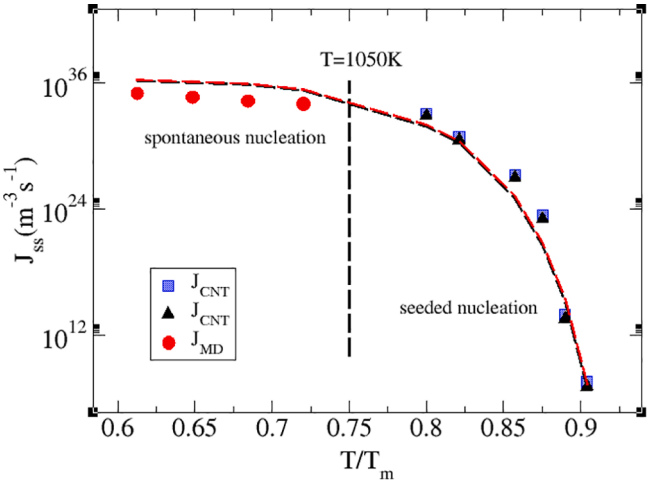

Fig. 5. Nucleation rate versus scaled temperature. The black triangles refer to nucleation rates calculated from the MD results for N^*, T_m, $\rho_f(T^*)$, $D^+(T^*)$ and $\Delta\mu$ (Eq. (5)). The blue squares are the nucleation rates calculated from N^*, T_m, $\rho_f(T^*)$, $D^+(T^*)$ and $\Delta\mu$ (Eq. (6)), both without any adjustable parameter. The red circles refer to spontaneous nucleation rates obtained using the mean lifetime method by $J_{MD} = 1/(\tau V)$. The black and red dashed lines show the $J_{ss}(T)$ extrapolated from the seeded nucleation region to the spontaneous nucleation region using the $N^*(T)$, $\rho_f(T)$, $\Delta\mu(T)$, and $D^+(T)$ via the CNT Eq. (4).

not differ from the $J_{CNT}(T)$ computed using Eq. (5) for $\Delta\mu$.

In the next section, we will obtain the steady-state nucleation rate, J_{ss}, by MD using the mean lifetime passage method and the results will be extrapolated to the seeded nucleation region using the CNT in an inverse way as done above.

4.3. Nucleation rates obtained directly by the mean lifetime method

In the deep supercooling regime, i.e. $T = (0.61 - 0.72)T_m$, spontaneous nucleation occurs within our MD time scales. Fig. 6 shows representative snapshots of the atomistic configuration as a function of time for three temperatures and five times. The OVITO software [69] was used to analyze the local environment of each particle. A common neighbor analysis [27,70] routine of the OVITO was used to identify the local environments of the particles. Particles that belong to the crystal nucleus (zinc-blende structure, i.e., an fcc lattice with two atoms in the base) are shown in green, whereas "amorphous" particles are shown in grey. To count the number of solid-like atoms, we calculated the q_6 order parameter as explained in Section 4.2.1. Fig. 7 shows the number of solid-like atoms as a function of time for six independent samples. Because nucleation is inherently a stochastic process, nuclei are born at different times and places in each sample. The onset time when the number of solid-like atoms start to grow, τ, was averaged over fifteen independent initial configurations at each temperature, $T = 1000, 950,$ 900 and $850K$. At each temperature, the volume of the simulation box size and τ were substituted into $J_{MD} = 1/(\tau V)$ to obtain nucleation rates. They were shown in Figs. 5 and 10 by red circles. The J_{MD} varies in the range, $(10^{33} - 10^{35})m^{-3}s^{-1}$, which are comparable to the values obtained by the same method for supercooled SiO_2 [23], BaS [27] and LJ [19].

After determining the nucleation rates, we calculated the value of γ by two distinct procedures explained in Section 2. In the first procedure, we assumed γ as a free fitting parameter obtained by a linear fit of $Ln[\frac{J\sqrt{T}}{D(T)}]$ versus $1/(T{\rho_s}^2\Delta\mu^2)$. The average of the self-diffusion coefficients of the Zn and Se atoms was used for calculating $D(T)$. From the fitting procedure, the average interfacial free energy was $\gamma = 0.132J/m^2$ when Eq. (5) was used for calculating $1/(T{\rho_s}^2\Delta\mu^2)$, and $\gamma = 0.131J/m^2$ when Eq. (6) was used. This average interfacial free energy for ZnSe is in good agreement with the $\gamma_{avg} = 0.127J/m^2$ calculated in Section 4.2.4 and has the same order of magnitude as the typical values reported from the

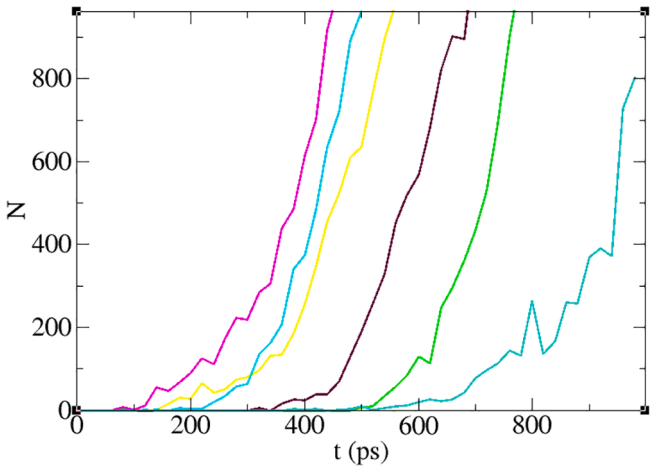

Fig. 7. Number of solid-like atoms determined via calculating the q_6 order parameter, as a function of time at $T = 950K$ for six samples. Each line corresponds to a specific sample. To get the average birth time, τ, the onset times when the number of atoms in the nucleus, N, starts to grow were averaged over fifteen independent initial configurations.

homogeneous nucleation analyses in BaS, $\gamma = 0.131J/m^2$ [27], oxide glasses $(0.10 < \gamma < 0.25J/m^2)$ [71] and a metallic system $\gamma = 0.17J/m^2$ [34].

Fig. 8 shows the $Ln[\frac{J\sqrt{T}}{D(T)}]$ as a function of $1/(T{\rho_s}^2\Delta\mu^2)$. Knowing the average value of γ, by substituting $D(T)$, γ, $\Delta\mu$ (from Eq. (5) or (6)) and λ into Eq. (9), we extrapolated the J_{MD} to the moderate supercooling regime. The result of the extrapolation is shown in Fig. 10 with red and green dashed lines. For the red dashed line, we used Eq. (5) to calculate $\Delta\mu$, whereas for the green dashed line we used Eq. (6).

In the second way, we obtained the values of γ at each temperature $T = 1000, 950, 900$ and $850K$ by substituting J_{MD}, T_m, λ, $D(T)$, $\Delta\mu(T)$ into Eq. (9), and fitted the resulting data with a linear function $\gamma = a + bT$. The calculated values of γ were shown in Fig. 9 by red circles and is in the range $\gamma = (0.123 - 0.126)J/m^2$. The red dashed line refers to the linear fit to data shown by the circles. The value of γ extrapolated from the spontaneous nucleation regime to the seeded nucleation regime lies within the values calculated from the seeding method. The temperature dependence of γ is very weak. By substituting the $\gamma(T)$, λ, $D(T)$ and $\Delta\mu(T)$

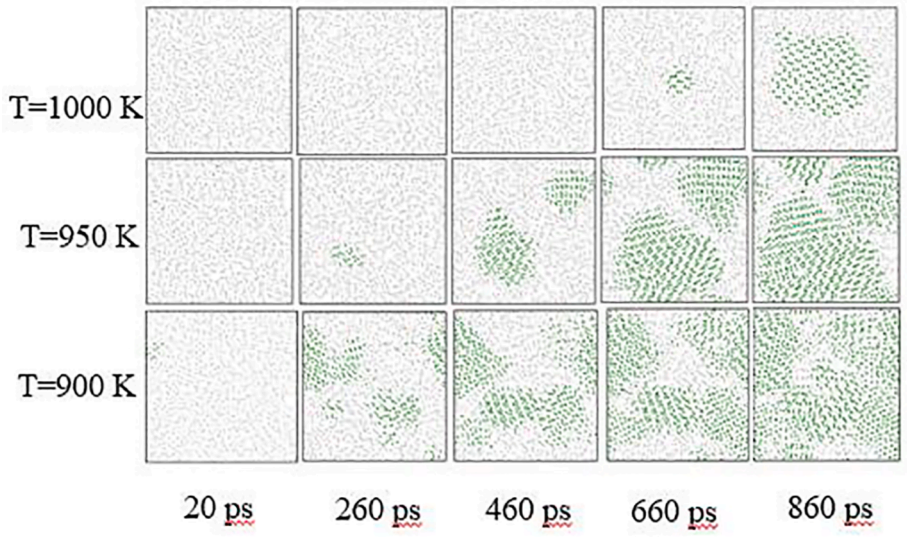

Fig. 6. Atomistic configuration as a function of time for three temperatures and five times. The common neighbor analysis shows the beginning of crystal nucleation and growth (green regions). For this particular ample at $T = 1000K$ in this particular sample, a nucleus appears after around $660ps$. However, this time decreases to $20ps$ at $T = 900K$.

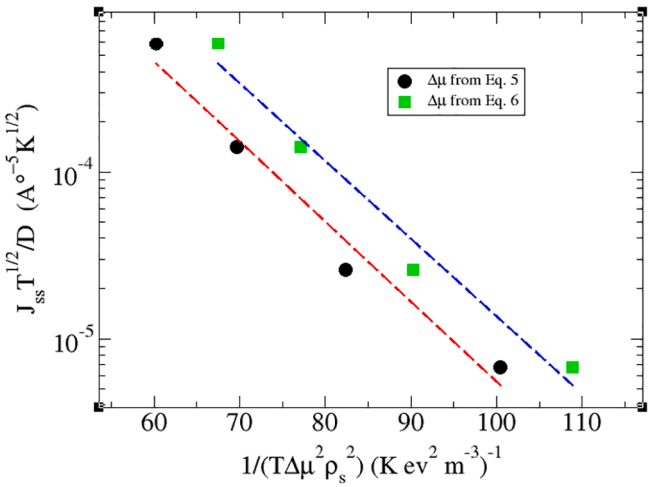

Fig. 8. Linearized nucleation rate plot: $\ln[J\sqrt{T}/D]$ as a function of $1/(T\rho_s{}^2\Delta\mu^2)$. We used Eq. (5) (circles) and Eq. (6) (squares) to determine $1/(T\rho_s{}^2\Delta\mu^2)$. The dashed lines show the fits using the CNT Eq. (9). From the slope of the fitted lines we estimated the interfacial free energy. The value obtained from the red line is $\gamma = 0.132J/m^2$, whereas from the blue line $\gamma = 0.131J/m^2$.

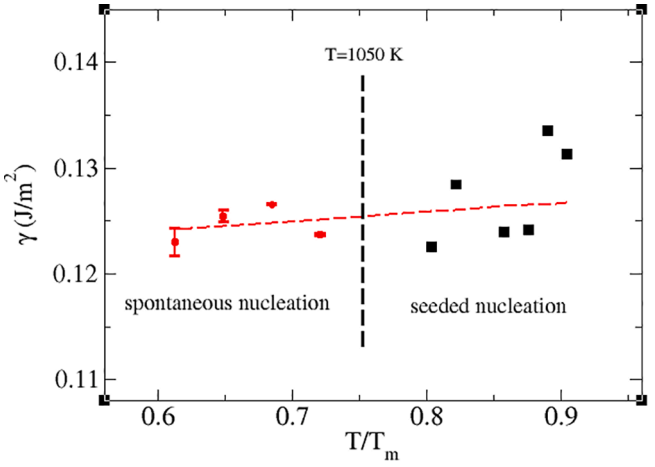

Fig. 9. Interfacial free energy versus supercooling T/T_m. The red circles refer to the values of γ calculated from Eq. (9) by using the values of J_{MD}, T_m, $D(T)$, λ and $\Delta\mu$ from Eq. (5). The black squares are the values of γ calculated in Section 4.2.4 from MD data of N^* and ρ_s and $\Delta\mu$ from Eq. (5) obtained via the seeding method using Eq. (3). The red dashed line shows a linear fit to the circles, extrapolated from spontaneous nucleation to the seeded nucleation regime.

into Eq. (9) we extrapolated $J_{MD}(T)$ from the spontaneous nucleation regime to the seeded nucleation regime. The result of this extrapolation is shown in Fig. 10 by a pink line. By substituting the $\gamma(T)$, $D(T)$ and λ in the pre-factor term of Eq. (9) i.e. $J_0 = \sqrt{\frac{\gamma}{k_B T}}\frac{D(T)}{\lambda^4}$, we obtained the kinetic pre-factors, which vary in the range of 10^{37} to $10^{38} m^{-3}s^{-1}$ for the temperature range $T = (0.61 - 0.72)T_m$. The extrapolated nucleation rates to deeper supercoolings reveal a well-known feature, which is the tendency to decrease after reaching a maximum [72].

The spontaneous nucleation rates, J_{MD}, obtained by MD for ZnSe and other simple substances lie in the range of 10^{30} to $10^{35} m^{-3}s^{-1}$ [16,23,33,34,35,36]. The previous analyses of experimental homogenous nucleation in several oxide glass-formers, shows that the experimental results of J_{ss} span a range from 10^4 to $10^{20} m^{-3}s^{-1}$ [71]. They are many orders of magnitude smaller than the theoretical values for these substances. One of the reasons for this discrepancy may be due to the procedure of calculating $D(T)$. In experiments, usually the Stokes-

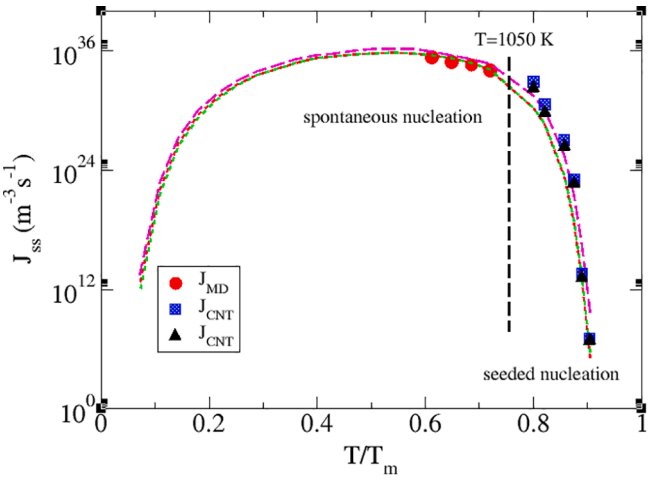

Fig. 10. Nucleation rate versus scaled temperature. The red circles refer to the steady-state nucleation rates obtained by the mean lifetime method from $J_{MD} = 1/(\tau V)$. The black triangles are the nucleation rates calculated from the MD results of N^*, T_m, ρ_f, D^+ and $\Delta\mu$ (Eq. (5)) via the CNT Eq. (4). The blue squares were calculated from MD results for N^*, T_m, ρ_f, D, λ, and $\Delta\mu$ (Eq. (5)) via the CNT Eq. (9). The red and green dashed lines refer to the J_{MD} extrapolated from the spontaneous nucleation regime to the seeded nucleation regime by substituting D, $\rho_f(T)$, $\Delta\mu$, from Eq. (5) and (6) and the average value of $\gamma = 0.132J/m^2$ when Eq. (5) was used for calculating $1/(T\rho_s{}^2\Delta\mu^2)$, and $\gamma = 0.131J/m^2$ when Eq. (6) was used, into the CNT Eq. (9) respectively. The pink line refers to extrapolated $J_{MD}(T)$ from the spontaneous regime to the seeded nucleation regime by substituting $D, \Delta\mu(T), \lambda$ and the temperature dependence of $\gamma(T)$, into Eq. (9). The nucleation rate reaches a maximum and decreases at deep supercooling because of the reduced mobility (pre-factor effect) at low temperature.

Einstein-Eyring (SEE) equation is used, and the $D(T)$ are calculated from the experimental values of viscosity. However, numerous studies show [73,74,75] that the SEE relation might breakdown at deep supercoolings, $T < 1.2T_g$, where T_g is glass transition temperature, which would lead to an enormous discrepancy in the pre-exponential term. In this work, however we obtained $D(T)$ directly from the simulations. In future research, we will also determine the diffusion coefficients from viscosity (via MD) by using the SEE relation to compare it with the $D(T)$ determined here to test for a possible breakdown.

According to the CNT, the spherical critical nucleus radius can be calculated by $R^* = 2\gamma/(\rho_s\Delta\mu)$. From this relation by substituting ρ_s, $\Delta\mu$ from Eq. (5) and the calculated values of γ obtained from J_{MD}, T_m, λ, $D(T)$, $\Delta\mu(T)$ via Eq. (9), R^* was calculated at four temperatures and the results are shown in the inset of Fig. 4 by green circles . From R^* we evaluated the N^* from the relation $N^* = \rho_s(4\pi R^{*3}/3)$. The results are shown by green circles in Fig. 4.

We also calculated $\frac{W^*}{k_B T}$ by substituting the calculated values of N^* and $\Delta\mu$ from Eq. (5) into Eq. (2). $\frac{W^*}{k_B T} = 5.4 - 9.3$ for temperature range $T = (0.61 - 0.72)T_m$. Using the temperature dependence γ, and $\Delta\mu$ from Eq. (5) by substituting them into Eq. (2) and (3), we extrapolated $\frac{W^*}{k_B T}$ to moderate supercooling. $\frac{W^*}{k_B T}$ changes in the range $(17.4 - 68.1)$ in temperature range $T = (0.8 - 0.9)T_m$, which are in good agreement with the results of the seeding method, $(16.1 - 75.6)$.

5. Summary and conclusions

We used a robust inter-atomic potential to obtain the melting point, T_m, the enthalpy of melting, Δh_m, the specific heat difference at the melting point, $\Delta c_{p,m}$, the self-diffusion coefficient, $D(T)$, the critical nucleus size, $N^*(T)$, and the times to form the first critical nucleus, τ, at

several supercoolings from MD simulations. These quantities, combined with theoretically calculated values of the thermodynamic driving force, allowed us to obtain crystal nucleation rates, $J_{ss}(T)$, in two regions of supercooled ZnSe: i) brute-force values of $J_{MD}(T)$ at deep supercoolings for spontaneous nucleation; ii) calculated values by the CNT at moderate supercoolings for seeded nucleation.

The interfacial free energy, γ, obtained from the critical nucleus sizes resulting from the seeding method at moderate supercoolings, and calculated from J_{MD} at deep supercoolings shows a weak temperature dependence. This result corroborates previous reports for other materials and is in line with the Diffuse Interface Theory of Nucleation. The extrapolated values of $\gamma(T)$ obtained by the MD-mean lifetime method at deep supercoolings to shallow supercoolings cover the values of γ obtained from the CNT of the nucleation rates calculated by the seeding method. The smallest critical nucleus radius refers to the spontaneous nucleation region at $T = 0.72T_m$ is $R = 5A^o$, which corresponds to two unit cells.

The most relevant result is that the theoretical and simulated nucleation rates agree with each other. These extensive results for ZnSe corroborate previous MD simulations for Lennard-Jones, H_2O, NaCl, SiO_2, Ge and Ni, and reinforce the validity of the CNT.

CRediT authorship contribution statement

Leila Separdar: Formal analysis, Investigation, Writing - original draft, Writing - review & editing, Visualization, Funding acquisition. **José Pedro Rino:** Conceptualization, Methodology, Validation, Writing - review & editing, Supervision, Project administration. **Edgar Dutra Zanotto:** Validation, Formal analysis, Writing - review & editing, Supervision, Project administration.

Declaration of Competing Interest

The authors declare that they have no known competing financial interests or personal relationships that could have appeared to influence the work reported in this paper.

Acknowledgments

We would like to thank CNPq, Brazil and The São Paulo Research Foundation, FAPESP, Brazil (contract CEPID # 2013/007793-6) for funding this work, and for a postdoctoral fellowship to LS (Grant # 2019/09499-4). We are also grateful to Azat O. Tipeev and Luis G. V. Gonçalves for their thorough analysis of the manuscript and most useful suggestions. All MD simulations were carried out using the computer facilities at the Physics Department, Federal University of São Carlos, Brazil.

References

[1] V.P. Skripov, V.P. Koverda, Spontaneous crystallization of supercooled liquids, Nauka, Moscow, 1984.
[2] G.M. Torrie, J.P. Valleau, Monte Carlo free energy estimates using non-Boltzmann sampling: application to the sub-critical Lennard-Jones fluid, Chem. Phys. Lett. 28 (1974) 578–581.
[3] A. Laio, M. Parrinello, Escaping free-energy minima, Proc. Nat. Acad. Sci. USA 99 (2002) 12562–12566.
[4] T.S. Van Erp, D. Moroni, P.G. Bolhuis, A novel path sampling method for the calculation of rate constants, J. Chem. Phys. 118 (2003) 7762–7774.
[5] R.J. Allen, D. Frenkel, P.R. ten Wolde, Forward flux sampling-type schemes for simulating rare events: efficiency analysis, J. Chem. Phys. 124 (2006) 194111–194117.
[6] C. Dellago, P.G. Bolhuis, D. Chandler, Efficient transition path sampling: application to Lennard-Jones cluster rearrangements, J. Chem. Phys. 108 (1998) 9236–9245.
[7] X.M. Bai, M. Li, Calculation of solid-liquid interfacial free energy: A classical nucleation theory based approach, J. Chem. Phys. 124 (2006) 124707–124719.
[8] X.M. Bai, M. Li, Differences between solid superheating and liquid supercooling, J. Chem. Phys. 123 (2015) 151102–151106.
[9] B.C. Knott, V. Molinero, M.F. Doherty, B. Peters, Homogeneous Nucleation of Methane Hydrates: Unrealistic under Realistic Conditions, J. Am. Chem. Soc. 134 (48) (2012) 19544–19547.
[10] J.R. Espinosa, C. Vega, C. Valeriani, E. Sanz, Seeding approach to crystal nucleation, J. Chem. Phys. 144 (2016) 034501–034510.
[11] D.W. Oxtoby, Homogeneous nucleation: theory and experiment, J. Phys: Condens. Matter 4 (1992) 7627–7650.
[12] K.F. Kelton, A.L. Greer, Nucleation in condensed matter: applications in materials and biology, first ed., Pergamon, United Kingdom, 2010.
[13] D.W. Oxtoby, Density functional methods in the statistical mechanics of material, Annu. Rev. Mater. Res. 32 (2002) 39–52.
[14] P.R. ten Wolde, M.J. Ruiz Montero, D. Frenkel, Numerical calculation of the rate of crystal nucleation in a Lennard-Jones system at moderate undercooling, J. Chem. Phys. 104 (1996) 9932–9947.
[15] X.M. Bai, M. Li, Test of classical nucleation theory via molecular-dynamics simulation, J. Chem. Phys. 122 (2005) 224510–224513.
[16] S.E.M. Lundrigan, I. Saika-Voivod, Test of classical nucleation theory and mean first-passage time formalism on crystallization in the Lennard-Jones liquid, J. Chem. Phys. 131 (2009) 104503–104507.
[17] P.R. ten Wolde, M.J. Ruiz Montero, D. Frenkel, Numerical calculation of the rate of homogeneous gas–liquid nucleation in a Lennard-Jones system, J. Chem. Phys. 110 (1999) 1591–1599.
[18] V.G. Baidakov, A.O. Tipeev, Crystal nucleation and the solid-liquid interfacial free energy, J. Chem. Phys. 136 (2012) 074510–074519.
[19] V.G. Baidakov, K.R. Protsenko, Spontaneous crystallization of a supercooled Lennard-Jones liquid: molecular dynamics simulation, J. Phys. Chem. B 123 (2019) 8103–8112.
[20] S. Auer, D. Frenkel, Prediction of absolute crystal-nucleation rate in hard-sphere colloids, Nature 409 (2001) 1020–1023.
[21] J.R. Espinosa, E. Sanz, C. Valeriani, C. Vega, Homogeneous ice nucleation evaluated for several water models, J. Chem. Phys. 141 (2014) 18C529–18C543.
[22] L. Lupi, A. Hudait, B. Peters, M. Grünwald, R. Gotchy Mullen, A.H. Nguyen, V. Molinero, Role of stacking disorder in ice nucleation, Nature 551 (2017) 218–222.
[23] I. Saika-Voivod, P.H. Poole, R.K. Bowles, Test of classical nucleation theory on deeply supercooled high-pressure simulated silica, J. Chem. Phys. 124 (2006) 224709–224724.
[24] C. Valeriani, E. Sanz, D. Frenkel, Rate of homogeneous crystal nucleation in molten NaCl, J. Chem. Phys. 122 (2005) 194501–194507.
[25] N.E.R. Zimmermann, B. Vorselaars, D. Quigley, B. Peters, Nucleation of NaCl from aqueous solution: critical sizes, ion attachment kinetics, and rates, J. Am. Chem. Soc. 37 (2015) 13352–13361.
[26] A.O. Tipeev, E.D. Zanotto, J.P. Rino, Crystal nucleation kinetics in supercooled germanium: MD simulations versus experimental data, J. Phys. Chem. B 124 (36) (2020) 7979–7988.
[27] S.C.C. Prado, J.P. Rino, E.D. Zanotto, Successful test of the classical nucleation theory by molecular dynamic simulations of BaS, Comp. Mat. Sci. 161 (2019) 99–106.
[28] A.O. Tipeev, E.D. Zanotto, Nucleation kinetics in supercooled Ni50Ti50: Computer simulation data corroborate the validity of the Classical Nucleation Theory, J. Chem. Phys. Lett. 735 (2019) 136749–136754.
[29] Y. Sun, H. Song, F. Zhang, L. Yang, Z. Ye, M.I. Mendelev, C.Z. Wang, K.M. Ho, Overcoming the time limitation in molecular dynamics simulation of crystal nucleation: a persistent-embryo approach, Phys. Rev. Lett. 120 (2018) 085703–085708.
[30] E.D. Zanotto, P.F. James, Experimental tests of the classical nucleation theory for glasses, J. Non-Cryst. Solids 74 (1985) 373–394.
[31] G.F. Neilson, M.C. Weinberg, A test of classical nucleation theory: crystal nucleation of lithium disilicate glass, J. Non-Cryst. Solids 34 (1979) 137–147.
[32] A. Laaksonen, V. Talanquer, D.W. Oxtoby, Nucleation: measurements, theory, and atmospheric application, Annu. Rev. Phys. Chem. 46 (1995) 489–524.
[33] D.A. Nicholson, G.C. Rutledge, Analysis of nucleation using mean first-passage time data from molecular dynamics simulation, J. Chem. Phys. 144 (2016) 134105–134115.
[34] A. Mahata, M.A. Zaeem, M.I. Baskes, Understanding homogeneous nucleation in solidification of aluminum by molecular dynamics simulations, Model. Simul. Mater. Sc. 26 (2018) 025007–025039.
[35] Y. Shibuta, K. Oguchi, T. Takaki, M. Ohno, Homogeneous nucleation and microstructure evolution in million-atom molecular dynamics simulation, Sci. Rep. UK 5 (2015) 13534–13543.
[36] G.E. Norman, V.V. Pisarev, Molecular dynamics analysis of the crystallization of an overcooled aluminum melt, Russ. J. Phys. Chem. A 86 (2012) 1447–1452.
[37] J.K. Bording, J. Taftø, Molecular-dynamics simulation of growth of nanocrystals in an amorphous matrix, Phys. Rev. B 62 (2000) 8098–8103.
[38] K.K. Tanaka, K. Kawamura, H. Tanaka, K. Nakazawa, Tests of the homogeneous nucleation theory with molecular-dynamics simulations. I. Lennard-Jones molecules, J. Chem. Phys. 122 (2005) 184514–184524.
[39] G. Grebe, G. Roussos, H.J. Schulz, Cr2+ excitation levels in ZnSe and ZnS, J. Phys. C: Solid State Phys. 9 (1976) 4511–4516.
[40] S. Guha, Zink Selenide, Encyclopedia of Materials: Science and Technology, second ed., 9894, 2001.
[41] S. Adachi, T. Taguchi, Optical properties of ZnSe, Phys. Rev. B 43 (1991) 9569–9577.
[42] A.S. Hassanien, K.A. Aly, A. Akl Alaa, Study of optical properties of thermally evaporated ZnSe thin films annealed at different pulsed laser powers, J. Alloys. Compounds 685 (2016) 733–742.

[43] M.A. Abdel-Rahim, M.M. Hafiz, A.E.B. Alwany, The effect of composition on structural and optical properties of ZnSe alloys, Optics Laser Technol. 47 (2013) 88–94.
[44] K.F. Kelton, Crystal Nucleation in liquids and glasses, Solid State Phys. 45 (1991) 75–177.
[45] I.S. Gutzow, J.W.P. Schmelzer, The Vitreous State: Thermodynamics, Structure, Rheology, and Crystallization, second ed., Springer, Heidelberg, Germany, 2013.
[46] J.W.P. Schmelzer, A.S. Abyzov, V.G. Baidakov, Entropy and the tolman parameter in nucleation theory, Entropy 21 (2019) 670–715.
[47] J.W.P. Schmelzer, A.S. Abyzov, Crystallization of glass-forming liquids: Thermodynamic driving force, J. Non-Cryst. Solids 449 (2016) 41–49.
[48] J.Q. Broughton, G.H. Gilmer, Molecular dynamics investigation of the crystal–fluid interface. VI. Excess surface free energies of crystal–liquid systems, J. Chem. Phys. 84 (1986) 5759–5768.
[49] J.J. Hoyt, M. Asta, A. Karma, Method for computing the anisotropy of the solid-liquid interfacial free energy, Phys. Rev. Lett. 86 (2001) 5530–5533.
[50] S. Angioletti-Uberti, M. Ceriotti, P.D. Lee, M.W. Finnis, Solid-liquid interface free energy through metadynamics simulations, Phys. Rev. B 81 (2010) 125416–125427.
[51] S. Auer, D. Frenkel, Numerical prediction of absolute crystallization rates in hard-sphere colloids, J. Chem. Phys. 120 (2004) 3015–3029.
[52] A.O. Tipeev, E.D. Zanotto, J.P. Rino, Diffusivity, interfacial free energy, and Crystal nucleation in a supercooled Lennard-Jones liquid, J. Phys. Chem. C 122 (2018) 28884–28894.
[53] J.W.P. Schmelzer, V.M. Fokin, A.S. Abyzov, Crystallization of glass: what we know, what we need to know, Int. J. Appl. Glass Sci. 7 (2016) 253–261.
[54] W.A. Harrison, Electronic structure and the properties of solids: the physics of the chemical bonds, San Francisco (1980).
[55] H. Karzel, W. Potzel, M. Köfferlein, W. Schiessl, M. Steiner, U. Hiller, G.M. Kalvius, D.W. Mitchell, T.P. Das, P. Blaha, K. Schwarz, M.P. Pasternak, Lattice dynamics and hyperfine interactions in ZnO and ZnSe at high external pressures, Phys. Rev. B 53 (1996) 11425–11438.
[56] D.R. Lide, Handbook of Chemistry and Physics, CRC Press Inc., New York, 1995.
[57] S.J. Plimpton, Fast parallel algorithms for short-range molecular dynamics, Comp. Phys. 117 (1995) 1–43.
[58] S.N. Luo, A. Strachan, D.C. Swift, Nonequilibrium melting and crystallization of a model Lennard-Jones system, J. Chem. Phys. 120 (2004) 11640–11649.
[59] S.N. Luo, T.J. Ahrens, Maximum superheating and undercooling: Systematics, molecular dynamics simulations, and dynamic experiments, Phys. Rev. B 68 (2003) 134206–134217.
[60] E.T. Chen, R.N. Barnett, U. Landmann, Crystal-melt and melt-vapor interfaces of nickel, Phys. Rev. B 40 (1989) 924–932.
[61] C.I. Ribeiro-Silva, J.P. Rino, L.G.V. Gonçalves, A. Picinin, An effective interaction potential for gallium phosphide, J. Phys.: Condens. Matter 23 (2011) 055801–055810.
[62] W. Zhang, Y. Peng, Z.h. Liu, Molecular dynamics simulations of the melting curve of NiAl alloy under pressure, AIP Advances 4 (2014) 057110–057123.
[63] P. Rudolph, N. Schtifer, T. Fukuda, Crystal growth of ZnSe from the melt, Mater. Sci. Eng. R 15 (1995) 85–133.
[64] P.J. Steinhardt, D.R. Nelson, M. Ronchetti, Bond-orientational order in liquids and glasses, Phys. Rev. B 28 (1983) 784–805.
[65] P.R. ten Wolde, D. Frenkel, Homogeneous nucleation and the Ostwald step rule, Chem. Phys. 1 (1999) 2191–2196.
[66] N.E.R. Zimmermann, B. Vorselaars, J.R. Espinosa, D. Quigley, W.R. Smith, E. Sanz, C. Vega, B. Peters, NaCl nucleation from brine in seeded simulations: Sources of uncertainty in rate estimates, J. Chem. Phys. 148 (2018) 222838–222848.
[67] J.W.P. Schmelzer, A.S. Abyzov, Crystallization of glass-forming liquids: specific surface energy, J. Chem. Phys. 145 (2016) 064512–064522.
[68] P.M. Hijes, J.R. Espinosa, E. Sanz, C. Vega, Interfacial free energy of a liquid-solid interface: its change with curvature, J. Chem. Phys. 151 (2019) 144501–144511.
[69] A. Stukowski, Visualization and analysis of atomistic simulation data with OVITO the open visualization tool, Model. Simul. Mater. Sci. Eng. 18 (2010) 015012–015020.
[70] H. Tsuzuki, P.S. Branicio, J.P. Rino, Structural characterization of deformed crystals by analysis of common atomic neighborhood, Comput. Phys. Commun. 177 (2007) 518–523.
[71] V.M. Fokin, E.D. Zanotto, N.S. Yuritsyn, J.W.P. Schmelzer, Homogeneous crystal nucleation in silicate glasses: a 40 years perspective, J. Non-Cryst. Solids 352 (2006) 2681–2714.
[72] E.B. Moore, V. Molinero, Structural transformation in supercooled water controls the crystallization rate of ice, Nature 479 (2011) 506–508.
[73] G. Tarjus, D. Kivelson, Breakdown of the Stokes-Einstein relation in supercooled liquids, J. Chem. Phys. 103 (1995) 3071–3073.
[74] S.K. Kumar, G. Szamel, J.F. Douglas, Nature of the breakdown in the Stokes-Einstein relationship in a hard sphere fluid, J. Chem. Phys. 124 (2006) 214501–214507.
[75] M. Cappelezzo, C.A. Capellari, S.H. Pezzin, L.A.F. Coelho, Stokes-Einstein relation for pure simple Fluids, J. Chem. Phys. 126 (2007) 224516–224521.